


SCIENTIFIC REPORTS



OPEN

Mesoporous 3C-SiC Hollow Fibers

Yangwen Liu^{1,2}, Huilin Hou², Xinbo He¹ & Weiyu Yang^{1,2} 

In the present work, for the first time, we reported the exploration of mesoporous 3C-SiC hollow fibers via single-spinneret electrospinning of polyureasilazane (PSN) and polyvinylpyrrolidone (PVP) solution followed by high-temperature pyrolysis treatment. The resultant products were characterized by X-ray diffraction (XRD), field emission scanning electron microscopy (FESEM), high-resolution transmission electron microscopy (HRTEM) and N₂ adsorption. The as-prepared hollow fibers with totally mesoporous walls were uniformly sized in diameter and high purity in morphology. They were composed of single-crystalline 3C-SiC nanoparticles with a surface area of 21.75 m²/g and average pore diameter of ~34 nm. The PSN concentration played a determined role on the formation of hollow fibers rather than the conventional solid counterparts, enabling their growth in a tunable manner. A possible mechanism was proposed for the formation of mesoporous SiC hollow fiber.

Porous silicon carbide (SiC) has attracted wide attention in many fields of energy production and environmental protection such as photocatalysts, catalyst supports, water purification, and thermal insulators, due to its superior mechanical properties, high thermal conductivity, low thermal-expansion coefficient, and good thermal-shock resistance, as well as its robust chemical stability and low electron affinity^{1–5}. Up to date, many efforts have been put into the production of porous SiC nanostructures through different strategies^{6–14}.

Electrospinning is a promising, low cost, and facile technique that has gained numerous and continuous interest, because of its capability and feasibility for mass production of organic/inorganic fibers with high qualities from polymer with diameters ranged from tens of nanometers to several micrometers^{15–21}, offering considerable interest for many applications, such as catalysts, nanoparticle carriers in controlled release, nanofibrous membranes or filters, and electronic sensors^{22–27}. By virtue of the simplicity and versatility of this technique assisted by subsequent carbothermal reduction, SiC dense/solid fibers/wires have been successfully generated^{28–31}. Most recently, there are growing interest for fabrication of nanoporous SiC hollow fibers^{32–34}, to enhance their properties and applications by increasing the surface areas and porosities. However, to the best of our knowledge, there are scarce works reported on the growth of hollow SiC fibers with high purity via single-spinneret electrospinning.

Herein, we report the exploration of mesoporous SiC hollow fibers via single-spinneret electrospinning of polyureasilazane (PSN) and polyvinylpyrrolidone (PVP), followed by high-temperature pyrolysis. We mainly focus on two points in current work: i) to realize the preparation of hollow SiC fibers with totally mesoporous walls; ii) to make the growth of the hollow fibers with uniform size in diameter and high purity in morphology in a tunable manner. It is promising that this work would inspire the study of mesoporous SiC hollow fibers with high surface area, which could have some potential applications to be utilized as catalyst supports and photocatalysts.

Experimental Procedure

Raw materials. Polyureasilazane (PSN, Ceraset, Kion Corporation, USA), Polyvinylpyrrolidone (PVP, $M_w \approx 30000$, Qurchem, Sinopharm Chemical Reagent Co., Ltd, Shanghai, China), absolute ethyl alcohol, hydrofluoric acid (HF) and hydrochloric acid (HCl) were commercially available, which were directly used as received without further treatment.

Preparation of mesoporous SiC hollow fibers. In a typical experimental procedure, the raw materials of 1.2 g PVP and 1.6 g PSN were firstly dissolved in 3.5 g absolute ethyl alcohol with stirring vigorously for 6 h. The resultant precursor microemulsions were transferred into a plastic syringe with a stainless steel nozzle (anode, diameter: 0.2 mm). The tip of the stainless steel nozzle was placed in front of a metal cathode (collector) with a fixed distance of 20 cm between the nozzle and the collector. An electrical potential of 16 kV was applied for electrospinning precursor fibers. The as-spun polymer fibers were located in a petri dish, which were dried in an oven at 80 °C for 4 h. Then the as-spun PVP/PSN fibers were cured at 200 °C for 2 h in air with a heating rate of 10 °C/min from room temperature (RT) to 100 °C, and then up to the desired temperature of 200 °C at 1 °C/min. Subsequently, the PVP/

¹Institute for Advanced Materials and Technology, University of Science and Technology Beijing, Beijing, 100083, P.R. China. ²Institute of Materials, Ningbo University of Technology, Ningbo City, 315016, P.R. China. Correspondence and requests for materials should be addressed to X.H. (email: xb_he@163.com) or W.Y. (email: weiyuyang@tsinghua.org.cn)

Sample	PVP (g)	PSN (g)	Alcohol (g)	PSN (wt.%)	S_{BET} (m ² /g)
A	1.2	0.8	3.5	14.5	16.57
B	1.2	1.0	3.5	17.5	20.42
C	1.2	1.2	3.5	20.3	15.45
D	1.2	1.4	3.5	23	20.34
E	1.2	1.6	3.5	25.4	21.75

Table 1. Compositions of five solutions used for electrospinning polymer precursor fibers and corresponding BET specific surface areas of pyrolyzed products.

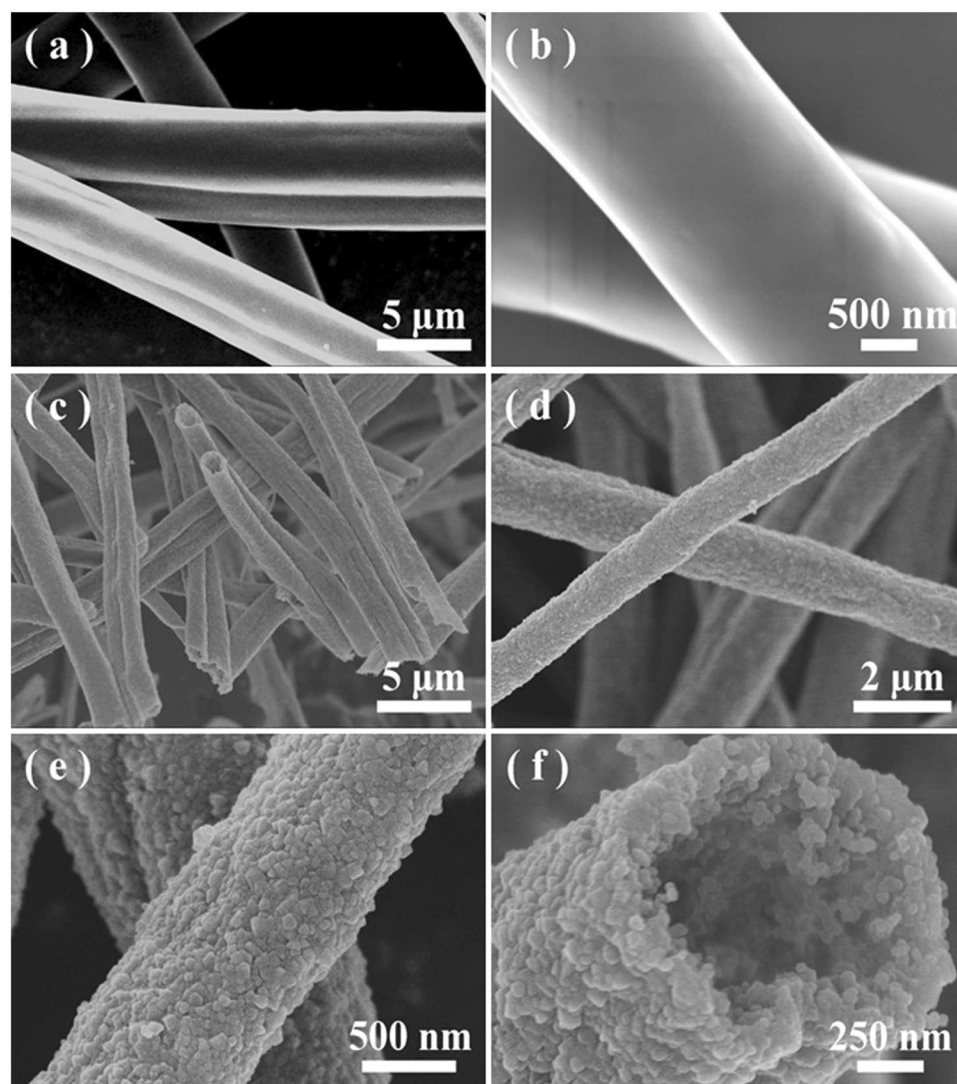


Figure 1. (a and b) Typical SEM images of the as-spun PVP/PSN fibers of Sample E. (c and d) Typical SEM images of the pyrolyzed products under different magnifications. (e) Representative SEM images of the surface structures of the as-fabricated mesoporous SiC hollow fibers. (f) A representative SEM image showing the fracture surface of the mesoporous hollow fibers.

PSN fibers were located in an Al₂O₃ crucible to be pyrolyzed in a graphite-heater furnace under flowing Ar (100 sccm, 99.9%, 0.1 MPa). The pyrolysis procedure was heated up to the desired temperature of 1400 °C with a heating rate of 10 °C/min, and maintained there for 1 h. After the furnace was cooled down to RT, the as-prepared product was collected. The raw product was purified by air calcination at 700 °C for 4 h to eliminate the redundant carbons. Finally, the SiO₂ layer existed around the surface of SiC fibers were removed by treatment with the mixed acid for 12 h, which are composed by 10 vol% HF + 10 vol% HCl + 80 vol% H₂O. The sample was then leached with distilled water until the pH maintained to ~7. For comparison, five solutions were prepared with different PSN contents, as shown in Table 1. The obtained products were referred to Sample A–E, respectively.

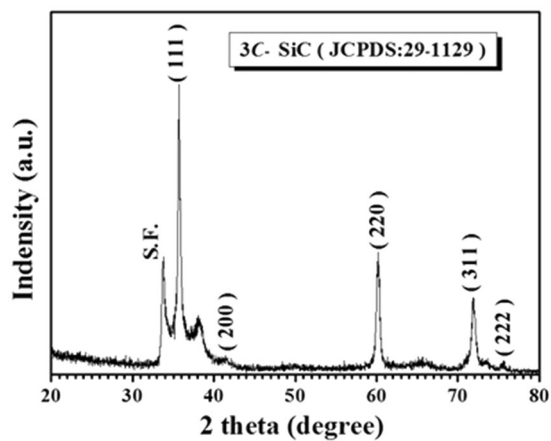


Figure 2. Representative XRD pattern recorded from Sample E after pyrolyzation at 1400 °C for 1 h.

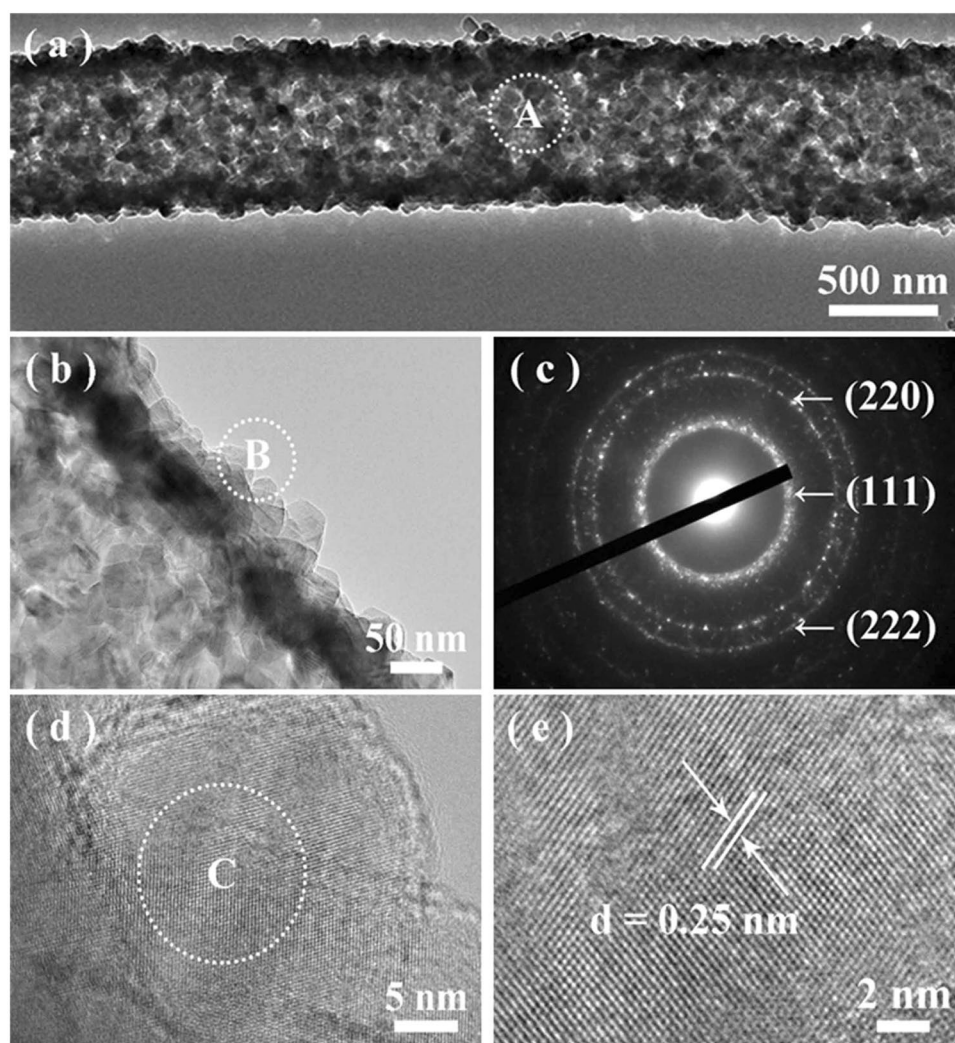


Figure 3. (a and b) Typical TEM images of a single SiC fiber from Sample E under different magnifications. (c) A typical SAED pattern recorded from the marked area of A in part a. (d) Typical HRTEM image obtained from a single nanoparticle recorded from the marked area of B in part b. (e) An enlarged HRTEM image recorded from the marked area of C in part d.

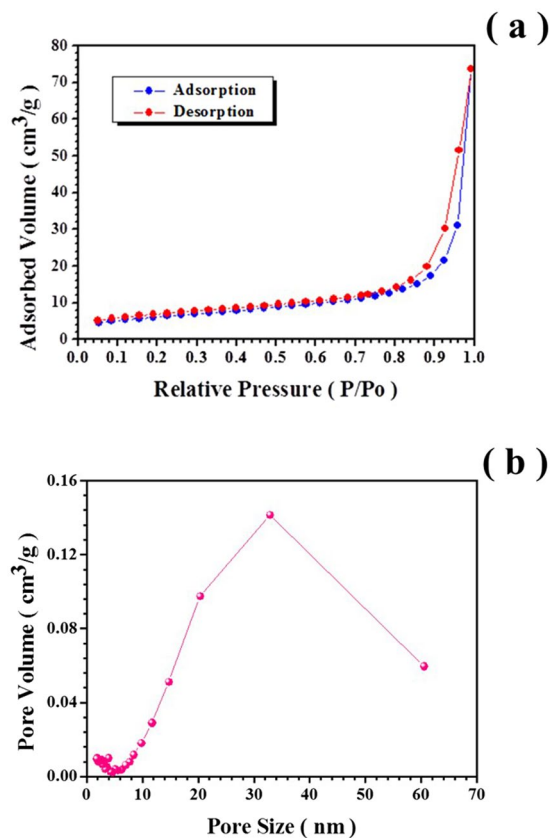


Figure 4. (a) Nitrogen adsorption-desorption isotherm curve of Sample E. (b) Pore size distribution curve of Sample E.

Structural characterization. The obtained products were characterized with X-ray powder diffraction (XRD, D8 Advance, Bruker, Germany) with Cu K α radiation ($\lambda = 1.5406 \text{ \AA}$), field emission scanning electron microscopy (FESEM, S-4800, Hitachi, Japan), and high-resolution transmission electron microscopy (HRTEM, JEM-2010F, JEOL, Japan) equipped with energy dispersive X-ray spectroscopy (EDX, Quantax-STEM, Bruker, Germany). The porous properties of the as-prepared mesoporous fibers were characterized using N₂ adsorption at $-195.8 \text{ }^\circ\text{C}$ on a specific surface area and porosity analyzer (ASAP 2020HD88, Micromeritics, USA).

Results and Discussion

SEM was firstly employed to study the morphology and microstructure of the precursor fibers of Sample E. The resultant precursor fibers (Fig. 1(a,b)) are continuous with the diameters in the range of $2\sim 4.5 \mu\text{m}$ with a smooth surface and typical length up to several hundred of millimeters. Figure 1(c–f) are the typical SEM images of the corresponding pyrolyzed products under different magnifications and views. It seems that the long continuous precursor fibers have been converted into hollow structures with the diameters reduced to $1\sim 2 \mu\text{m}$. The resultant fibers are uniform in diameter with a high purity in morphology. Figure 1(e,f) show the interior and external surface of the hollow fibers under different magnifications, respectively, which disclose that numerous pores exist on the surface and walls, representing that the as-prepared fibers are totally mesoporous. The formation of hollow and mesoporous structures is mainly attributed to the decomposition and removing of organics within the as-spun polymeric fibers.

Figure 2 presents the typical XRD pattern of the resultant hollow fibers of Sample E. The peak sets well match the phase of 3C-SiC (JCPDS, No. 29-1129), which can be attributed to the fact that SiC is more stable than Si_3N_4 , according to the Si–C–N ternary diagram at $1400 \text{ }^\circ\text{C}$ under an Ar atmosphere³⁵ (PSN and PVP composed mainly of Si, C, N, and H elements). The strong and sharp diffraction peaks indicate that the products are highly crystalline. A small peak ($2\theta = 33.8^\circ$) marked with S.F. can be ascribed to the stacking faults within the 3C-SiC structure³⁶. The stacking faults might reassemble the structures of other polytype phases of SiC such as α -SiC within the 3C-SiC matrix^{37, 38}. Accordingly, the minor peak ($2\theta = 38.2^\circ$) might be assigned to the diffraction of the (103) crystal plane of α -SiC.

TEM was further used to investigate the morphology and structural details of the hollow fiber, as shown in Fig. 3(a). In agreement with the SEM observations, the inner tunnel is clearly observed by the sharp contrast between SiC mesoporous wall and the hollow interior. The closer observation (Fig. 3b) presents that the fibers typically consist of irregular plate-like nanoparticles. The chemical compositions are identified by EDX under TEM recorded from a single fiber, suggesting that they mainly consist of Si and C, with a little amount of Al and O elements (the Cu signals are from the TEM copper grids) (Figure S1 in Supporting Information). The atomic

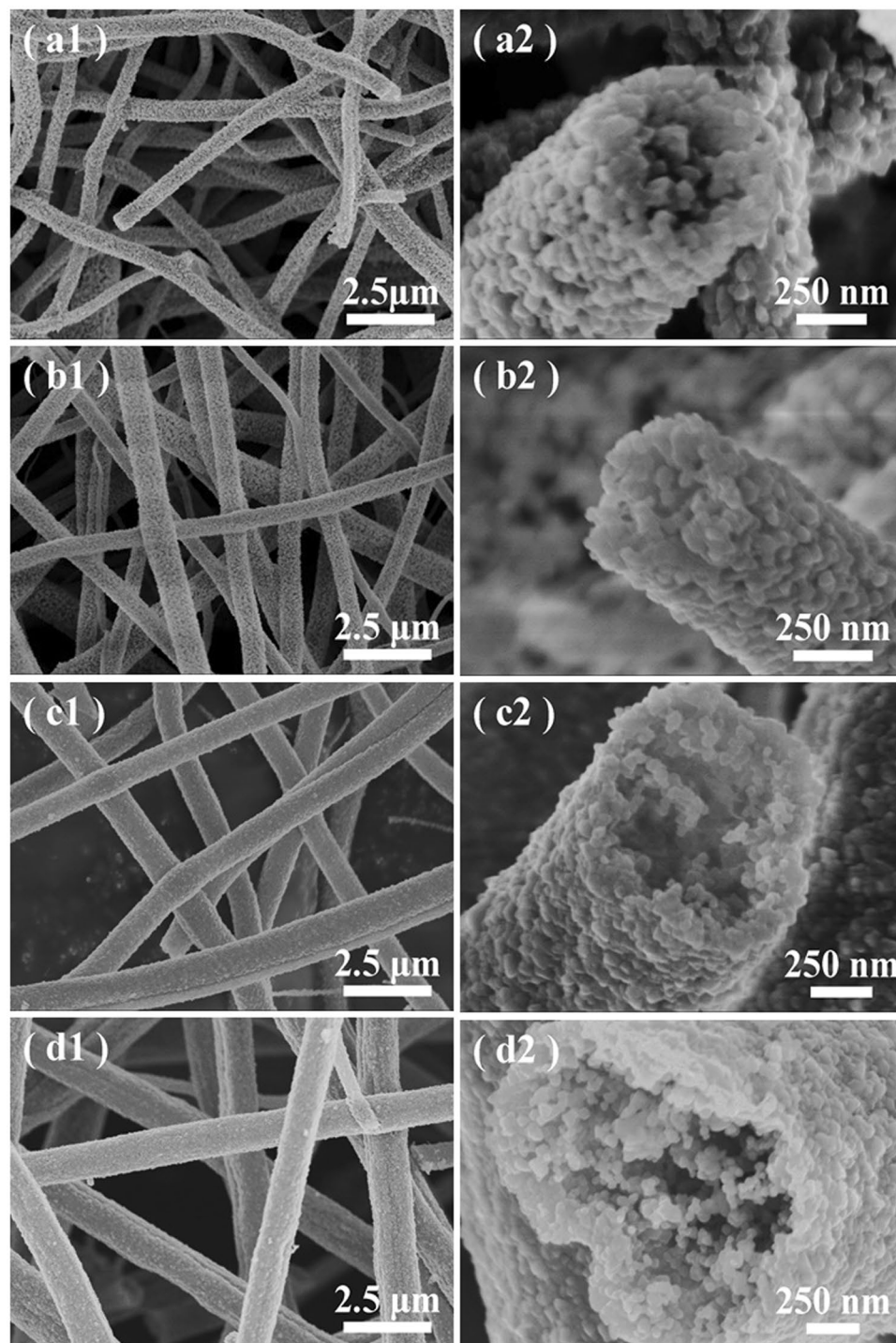


Figure 5. Typical SEM images of pyrolyzed products of Sample A (a1–a2), Sample B (b1–b2), Sample C (c1–c2), and Sample D (d1–d2) under different magnifications.

ratio of Si to C, within the experimental limit, is close to 1:1, suggesting the fibers are SiC. The detected Al and O elements should be attributed to the introduced impurities from the used Al_2O_3 crucible for the high-temperature pyrolysis treatment and the absorbed oxygen when the fibers were exposed in air, respectively. Figure 3c presents a typical selective area electron diffraction (SAED) pattern recorded from the whole fiber body (marked area of A in Fig. 3a), suggesting its polycrystalline nature with a high crystallinity. The diffraction spot rings could be sequentially indexed to be the (111), (220), and (222) crystal planes of 3C-SiC (JCPDS, No. 29–1129), further confirming that the resultant hollow fibers are of pure -SiC. Figure 3d and e present the representative HRTEM images recorded from a single particle, which are obtained from the marked area of B in Fig. 3b and c,

respectively, disclosing the single-crystalline nature of the nanoparticles. That is to say, the as-fabricated hollow SiC fibers are composed of single-crystalline nanoparticles.

The nitrogen adsorption measurements as shown in Fig. 4(a) reveal that the as-fabricated products exhibit the type IV isotherm behavior with H3 hysteresis, implying that the obtained hollow fibers are mesoporous with a BET surface area of 21.75 m²/g. According to the Barrett–Joyner–Halenda (BJH) pore size distribution analysis determined from the adsorption branches (Fig. 4(b)), the average BJH pore diameter is ~34 nm.

To disclose the growth of hollow SiC fibers, another four comparative experiments are carried out by adjusting the PSN contents and keeping the PVP and alcohol constant (Table 1). The experimental results suggest that all the pyrolyzed products of Sample A–E are of 3C-SiC phase (Fig. 2, Figure S2 in Supporting Information), implying that the change of the PSN contents has little influence on the phase formation of the final products. The BET specific areas of the hollow samples show a little change with the variation of the introduced PSN contents (Table 1, Figure S3 in Supporting Information). With a low concentration of PSN introduced in the raw materials (*i.e.*, Sample A and B), the conventional solid fibers would be formed (Fig. 5(a1,a2 and b1,b2)). Once the PSN contents is up to ~20 wt.% (*i.e.*, Sample C), the fibers with hollow interior seem to be formed. The growth of the hollow fibers could be accomplished with more and more PSN introduced into the raw materials (*i.e.*, Sample D and E, Figure 5(c1,c1 and d1,d2)). The diameters of the as-prepared fibers are increased with the more PSN concentrations, which could be mainly attributed to various viscosities and dielectric constant, since a larger diameter of the polymer fibers would be spun by increasing the viscosity of the solution (Table 1, Figure S4 in Supporting Information). It suggests that the PSN concentration plays a determined role on the formation of the hollow SiC fibers, enabling their growth in a controlled manner. In our case, the PSN concentration high up to 20 wt.% is necessary for the formation of hollow SiC nanofibers.

Based on the experimental results as mentioned above, the growth of mesoporous SiC hollow fibers is proposed as: i) The formation of the hollow interior. In regard to the Sample A–E, the only difference is the various PSN contents introduced within the raw materials. As compared to the initial diameter of the as-spun polymeric fibers, those of the pyrolyzed counterparts are often obviously shrunk, due to the elimination of the organics such as PVP within the polymeric fibers caused by the high-temperature treatment. As shown in Figs 1 and 5, with more PSN introduced, the diameter of the resultant SiC fibers is larger. This implies that the outlayer of inorganic SiC for the pyrolyzed fibers could be prior formed with a high enough PSN introduced to the raw materials (*i.e.*, with high enough Si contents from the PSN for the formation of SiC). The formed SiC outlayer might hinder the shrinkage of the fibers. Subsequently, the further elimination of the organics from the interior part of the polymeric fiber causes the formation of the hollowed interior; ii) The formation of the thoroughly mesoporous walls. It is mainly attributed to the selective evaporation/calcination mechanism^{23,30}, due to the two distinctively different thermal properties between PSN and PVP. It is known that the PSN mainly contains of Si, C, and N elements with a small amount of O (Figure S5 in Supporting Information), which would be converted into amorphous SiCN solids and can be thermally stable up to 1000 °C^{39,40}. However, the PVP is mainly composed of C, N, H, and O elements (Figure S5 in Supporting Information), which would be completely decomposed into vapor phases such as NH₃, CH₄, and CO₂ when heated up to ~500 °C^{41,42}. This is verified by the analysis of the thermal behaviors of as-spun PSN/PVP fibers from Sample E (Figure S6 in Supporting Information). Once subjected to be calcinated at high temperature, the PSN would be converted into inorganic SiC for constructing the walls of the hollow fibers, and the PVP would be completely decomposed into gas phases, making the creation of mesopores throughout the body of the fiber walls.

Conclusions

In summary, we have demonstrated the exploration of mesoporous SiC hollow fibers via single-spinneret electrospinning technique with the subsequent high-temperature pyrolysis treatment. The hollow SiC fibers with totally mesoporous walls are uniformly sized in diameter and high purity in morphology. They are composed of single-crystalline 3C-SiC nanoparticles with a surface area of 21.75 m²/g and average pore diameter of ~34 nm. It is found that the PSN concentration within the raw materials played a determined role on the formation of hollow fibers, making their growth in a tunable manner. The growth of the mesoporous SiC hollow fibers could be mainly attributed to the selective evaporation/calcination of PSN and PVP. The as-prepared mesoporous hollow fibers could have some potential applications in photocatalysts, catalyst supports and supercapacitor, owing to their light weight, high surface area as well as their hollow and mesoporous characteristics.

References

- Eddy, C. R. & Gaskill, D. K. Silicon Carbide as a Platform for Power Electronics. *Science* **324**, 1398–1400 (2009).
- Chen, S. *et al.* Highly flexible and robust N-doped SiC nanoneedle field emitters. *NPG Asia Mater.* **7** (2015).
- Casady, J. B. & Johnson, R. W. Status of silicon carbide (SiC) as a wide-bandgap semiconductor for high-temperature applications: A review. *Solid-State Electron* **39**, 1409–1422 (1996).
- Gao, F., Zheng, J., Wang, M., Wei, G. & Yang, W. Piezoresistance behaviors of p-type 6H-SiC nanowires. *Chem. Commun.* **47**, 11993–11995 (2011).
- Fan, J. Y., Wu, X. L. & Chu, P. K. Low-dimensional SiC nanostructures: Fabrication, luminescence, and electrical properties. *Prog. Mater. Sci.* **51**, 983–1031 (2006).
- Guo, X. Y. & Jin, G. Q. Pore-size control in the sol–gel synthesis of mesoporous silicon carbide. *Journal of Mater. Sci* **40**, 1301–1303 (2005).
- Shi, Y. F. *et al.* Highly Ordered Mesoporous Silicon Carbide Ceramics with Large Surface Areas and High Stability (pages 561–567). *Adv. Funct. Mater.* **16**, 561–567 (2006).
- Wang, B. *et al.* Mesoporous silicon carbide nanofibers with *in situ* embedded carbon for co-catalyst free photocatalytic hydrogen production. *Nano Res* **9**, 886–898 (2016).
- Yang, Z., Xia, Y. & Mokaya, R. High Surface Area Silicon Carbide Whiskers and Nanotubes Nanocast Using Mesoporous Silica. *Chem. Mater.* **16**, 3877–3884 (2004).

10. Kasinathan, K., Kennedy, J., Elayaperumal, M., Henini, M. & Malik, M. Photodegradation of organic pollutants RhB dye using UV simulated sunlight on ceria based TiO₂ nanomaterials for antibacterial applications. *Sci. Rep.* **6**, 38064 (2016).
11. Kaviyarasu, K. *et al.* Solution processing of CuSe quantum dots: Photocatalytic activity under RhB for UV and visible-light solar irradiation. *Mater. Sci. Eng., B* **210**, 1–9 (2016).
12. Kaviyarasu, K. *et al.* Photocatalytic activity of ZrO₂ doped lead dioxide nanocomposites: Investigation of structural and optical microscopy of RhB organic dye. *Appl. Surf. Sci.* (2016).
13. Kaviyarasu, K. *et al.* Synthesis and characterization studies of NiO nanorods for enhancing solar cell efficiency using photon upconversion materials. *Ceram. Int.* **42**, 8385–8394 (2016).
14. Kaviyarasu, K., Manikandan, E., Kennedy, J. & Maaza, M. A comparative study on the morphological features of highly ordered MgO:AgO nanocube arrays prepared via a hydrothermal method. *Rsc Adv* **5**, 82421–82428 (2015).
15. Agarwal, S., Greiner, A. & Wendorff, J. H. Functional materials by electrospinning of polymers. *Prog. Polym. Sci.* **38**, 963–991 (2013).
16. Li, D., Wang, Y. & Xia, Y. Electrospinning Nanofibers as Uniaxially Aligned Arrays and Layer-by-Layer Stacked Films. *Adv. Mater.* **16**, 361–366 (2004).
17. Szilágyi, I. M. *et al.* Photocatalytic Properties of WO₃/TiO₂ Core/Shell Nanofibers prepared by Electrospinning and Atomic Layer Deposition. *Chem. Vap. Deposition* **19**, 149–155 (2013).
18. Teo, W. E. & Ramakrishna, S. A review on electrospinning design and nanofibre assemblies. *Nanotechnology* **17**, R89–R106 (2006).
19. Huang, Z. M., Zhang, Y. Z., Kotaki, M. & Ramakrishna, S. A review on polymer nanofibers by electrospinning and their applications in nanocomposites. *Compos. Sci. Techn.* **63**, 2223–2253 (2003).
20. Bhardwaj, N. & Kundu, S. C. Electrospinning: A fascinating fiber fabrication technique. *Biotechnol. Adv.* **28**, 325–347 (2010).
21. Doshi, J. & Reneker, D. H. Electrospinning process and applications of electrospun fibers. *J. Electrostat.* **35**, 151–160 (1995).
22. Hou, H. *et al.* Fabrication of porous titanium dioxide fibers and their photocatalytic activity for hydrogen evolution. *Int. J. Hydrogen energy* **39**, 6837–6844 (2014).
23. Hou, H. *et al.* General strategy for fabricating thoroughly mesoporous nanofibers. *J. Am. Chem. Soc.* **136**, 16716–16719 (2014).
24. Kim, S. J., Nam, Y. S., Rhee, D. M., Park, H. S. & Park, W. H. Preparation and characterization of antimicrobial polycarbonate nanofibrous membrane. *Eur. Polym. J.* **43**, 3146–3152 (2007).
25. Komeil, N., Hossein, B., Amir, R., Mousavi, S. A. & Ali, K. Modeling and optimization of electrospun PAN nanofiber diameter using response surface methodology and artificial neural networks. *J. Appl. Polym. Sci.* **126**, 127–135 (2012).
26. Subbiah, T., Bhat, G. S., Tock, R. W., Parameswaran, S. & Ramkumar, S. S. Electrospinning of nanofibers. *J. Appl. Polym. Sci.* **96**, 557–569 (2005).
27. Zhan, S., Chen, D., Xiuling Jiao, A. & Tao, C. Long TiO₂ Hollow Fibers with Mesoporous Walls: Sol–Gel Combined Electrospun Fabrication and Photocatalytic Properties. *J. Phys. Chem. B* **110**, 11199–11204 (2006).
28. Li, J. *et al.* Single-crystalline nanowires of SiC synthesized by carbothermal reduction of electrospun PVP/TEOS composite fibres. *Nanotechnology* **18**, 363–372 (2007).
29. Choi, S. H., Youn, D. Y., Jo, S. M., Oh, S. G. & Kim, I. D. Micelle-Mediated Synthesis of Single-Crystalline β (3C)-SiC Fibers via Emulsion Electrospinning. *Acs Appl. Mater. Inter.* **3**, 1385–1389 (2011).
30. Hou, H. *et al.* Electrospinning 3C-SiC Mesoporous Fibers with High Purities and Well-Controlled Structures. *Cryst. Growth Des.* **12**, 536–539 (2012).
31. Zhou, J. Y., Chen, Z. Y., Zhou, M., Gao, X. P. & Xie, E. Q. SiC Nanorods Grown on Electrospun Nanofibers Using Tb as Catalyst: Fabrication, Characterization, and Photoluminescence Properties. *Nanoscale Res. Lett.* **4**, 814–819 (2009).
32. Lee, S. H., Yun, S. M., Sang, J. K., Park, S. J. & Lee, Y. S. Characterization of nanoporous β -SiC fiber complex prepared by electrospinning and carbothermal reduction. *Res. Chem. Intermed.* **36**, 731–742 (2010).
33. Lu, P., Huang, Q., Mukherjee, A. & Hsieh, Y. L. *Effects of polymer matrices to the formation of silicon carbide (SiC) nanoporous fibers and nanowires under carbothermal reduction.* (Foreign Languages Publishing House, 1955).
34. Piotr, K., Claudia Weidenthaler, A. & Stefan, K. SiC/MCM-48 and SiC/SBA-15 Nanocomposite Materials. *Chem. Mater.* **16**, 2869–2880 (2004).
35. Seifert, H. J., Peng, J., Lukas, H. L. & Aldinger, F. Phase equilibria and thermal analysis of Si–C–N ceramics. *ChemInform* **320**, 251–261 (2001).
36. Koumoto, K., Takeda, S., Pai, C. H., Sato, T. & Yanagida, H. High-Resolution Electron Microscopy Observations of Stacking Faults in β -SiC (pages 1985–1987). *J. Am. Ceram. Soc.* **72**, 1985–1987 (1989).
37. Zhang, L. *et al.* Ultraviolet photoluminescence from 3C-SiC nanorods. *Appl. Phys. Lett.* **89**, 143101–143103 (2006).
38. Carduner, K. R., Shinozaki, S. S., Rokosz, M. J., Peters, C. R. & Whalen, T. J. Characterization of β -silicon carbide by silicon-29 solid-state NMR, transmission electron microscopy, and powder X-ray diffraction. *J. Am. Ceram. Soc.* **73**, 2281–2286 (1990).
39. Li, Y. L. *et al.* Thermal cross-linking and pyrolytic conversion of poly(ureamethylvinyl)silazanes to silicon-based ceramics (pages 820–832). *Appl. Organomet. Chem* **15**, 820–832 (2001).
40. Todi, R. Investigation on RF sputter deposited SiCN thin Film for MEMS applications. *Mater. Sci. Eng., A* **368**, 103–108 (2004).
41. Kroke, E. *et al.* Silazane derived ceramics and related materials. *Materials. Sci. Eng., R* **26**, 97–199 (2000).
42. Loría-Bastarrachea, M. I. *et al.* A TG/FTIR study on the thermal degradation of poly(vinyl pyrrolidone). *J. Therm. Anal. Calorim.* **104**, 737–742 (2011).

Acknowledgements

This work was supported by National Natural Science Foundation of China (NSFC, Grant No. 51372122, 51372123 and 51274040) and the Fundamental Research Funds for the Central Universities (FRF-TP-10-003B).

Author Contributions

X.H. and W.Y. conceived and directed the experiments. Y.L. and H.H. performed the experiments. Y.L., X.H. and W.Y. co-wrote the manuscript. All authors discussed the results and helped for the preparation of the manuscript.

Additional Information

Supplementary information accompanies this paper at doi:10.1038/s41598-017-02147-8

Competing Interests: The authors declare that they have no competing interests.

Publisher's note: Springer Nature remains neutral with regard to jurisdictional claims in published maps and institutional affiliations.



Open Access This article is licensed under a Creative Commons Attribution 4.0 International License, which permits use, sharing, adaptation, distribution and reproduction in any medium or format, as long as you give appropriate credit to the original author(s) and the source, provide a link to the Creative Commons license, and indicate if changes were made. The images or other third party material in this

article are included in the article's Creative Commons license, unless indicated otherwise in a credit line to the material. If material is not included in the article's Creative Commons license and your intended use is not permitted by statutory regulation or exceeds the permitted use, you will need to obtain permission directly from the copyright holder. To view a copy of this license, visit <http://creativecommons.org/licenses/by/4.0/>.

© The Author(s) 2017